3D Stress Distribution Analysis around Blind-holes in Thin Plates Under Non-uniform Tension Loads

by, J. Carrera, J.E. Martínez and L. Ferrer

PhD, Professor of Mechanical and Industrial Engineering Division, Engineering Faculty, Universidad NacionalAutónoma de México, Distrito Federal, México.
PhD, PostgraduateDivision, EngineeringFaculty, Universidad Nacional Autónoma de México, Distrito Federal, México.
PhD, late Professor, Mechanical and Industrial EngineeringDivision, EngineeringFaculty, Universidad Nacional Autónoma de México, Distrito Federal, México

ABSTRACT.

A three-dimensional photo elasticity analysis and an interactive finite-element package were used in parallel to analyze the stress distribution on the root of blind-holes in thin plates. Experimental analysis was conducted via stress freezing method. The FEM analysis was performed with the ABAQUS commercial code using material properties obtained experimentally as input. The results showed that the maximum stress distribution occurred in three zones: the first one at the beginning of the blind-hole; the second one at the transition zone where the root begins his shape; and at the center of the root.These results are expected to improve blind-hole design according to its function. The combined use of experimental and numerical methods provides more information than each method taken alone. This information is essential when the relation between depth and thickness has to be taken into account. As shown here, the stresses near the free boundary are relevant for failure considerations, for example due to the presence of debris in thin plates or sheets. An analog statement can be made for blind-holes made to fasten metal sheets with bolts or hollows for human prosthesis.

KEY WORDS- Blind-hole, stress-freezing method, FEM, photoelasticity, stress concentration.

I. Introduction

In engineering practice the presence of holes, notches or any other geometry that causes stress concentration has been studied since Kirsch [1] in 1898. Problems with abrupt change of geometry in structural components are well known: stress concentration may be induced around the hole or notch, causing severe reductions of the strength and fatigue life of a structure. An important technical example of this situation is given when debris are present in laminating processes; such defects can be well modeled as blind holes. Many are the cases when the structural component has blind-holes created to fasten different parts of the component, or simply by design. The determination of the stress concentration around holes and notches was, and still is, one of the most common applications of 2D and 3D photoelasticity of machine elements design. In the literature, theoretical, experimental and numerical solutions were obtained for several cases where a circular hole has a particular function in thin or thick plates.Iancuet. al. [2] evaluated the stress distribution inside thick bolted plates along the bearing plane normal to theplate surface.

Their experimental and numerical results help them to develop an improved joint design.

Another stress distribution research in plates with circular holes was developed by Wang et. al. [3]. In their paper, they proposed a replaced superposition method to reconstruct experimental photoelastic fringe patterns of a near-surface circular hole.

Peindlet. al. [4] did an analysis of a total shoulder replacement system via photoelastic stress freezing. They showed that maximum stress occurred at the neck and at the component-bone interface beneath simulated PMMA inclusions on both axial and coronal planes. Those planes exhibit blind-holes for different depths and root-shapes due to the whole replacement system.

However, to the best of our knowledge, no experimental-numerical solution of the stress distribution around a blind-hole when a thin plate is under tension loads available in the literature. Figure 1 illustrates this point.

The purpose of this paper is three-fold. First to reproduce the boundary conditions required at the plate and develop a model whereby stress freezing method is used. Second, to analyze and acquire new information about maximal stresses along blind-hole's route and root. And third, to show how numerical results corroborate and support qualitative results from the experimental ones.

II. Mathematical statement of the problem

Consider a homogeneous, isotropic, elastic body $\Omega \subset \mathbb{R}^3$ at equilibrium define by $|x| < L$, $|y| < A$, $|z| < 2h$ where $L, A, h > 0$ are given. It contains a cylindrical blind-hole of radius a whose generators are perpendicular to the bounding planes and consists of two geometries, a cylinder

$$Cl = \{(x,y,z) | x^2 + y^2 \le a^2, 0 \le z \le c_1\}$$

and a semi-sphere SE

$$SE = \{(x,y,z) | x^2 + y^2 + (z - c_1)^2 \le r^2; c_1 \le z \le c_1 + r\}$$

so the body $\Omega = REC \setminus (Cl \cup SE)$, where REC is the rectangle of dimensions $L \times A \times t$.

For this particular study the plate has the dimensions: $L = 60 \text{ mm} (2.36 \text{ in}), A = 26 \text{ mm} (1 \text{ in}), a = 2.4 \text{ mm} (0.1 \text{ in}), r = 1.6 \text{ mm} (0.06 \text{ in}), t = 9.2 \text{ mm} (0.36 \text{ in})$.

Let the plate be subjected to a non-uniform tensile load along the x-axis and parallel to the bounding planes (Figure 1).
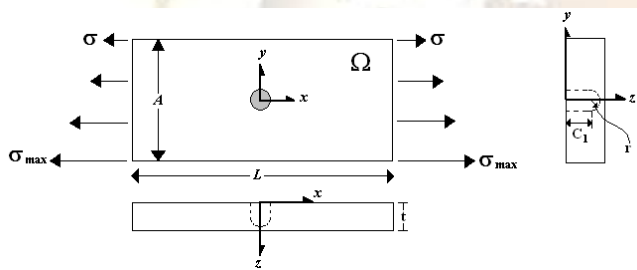

Figure 1 Geometrical configuration of a plate weakened by a circular blind-hole

The linear system of partial differential equations for the field **u**, **E** and **S** is

$$\left.\begin{aligned}
\mathbf{E}(\mathbb{p},t) &= \frac{1}{E}\left[(1+\nu)\mathbf{S}(\mathbb{p},t) - \nu(\mathrm{tr}\mathbf{S}(\mathbb{p},t))\mathbf{I}\right] \\
\mathbf{E}(\mathbb{p},t) &= \frac{1}{2}\left(\boldsymbol{\nabla}\mathbf{u}(\mathbb{p},t) + \boldsymbol{\nabla}\mathbf{u}(\mathbb{p},t)^{\mathrm{T}}\right) \\
\mathrm{Div}\mathbf{S}(\mathbb{p},t) &+ \mathbf{b_o}(\mathbb{p},t) = \rho_o \ddot{\mathbf{u}}(\mathbb{p},t)
\end{aligned}\right\} (1)$$

where **E** is called the infinitesimal strain field, **S** is the first Piola-Kirchhoff stress field, $\mathbf{b_o}$ is the body force, **u** is the displacement field and E, ν are called Young's modulus and Poisson's ratio respectively [5].

As to the boundary conditions, it is required that

$$at \qquad |x| = L: \frac{\partial \mathbf{u}(\mathbb{p},t)}{\partial \mathbf{n}} = f(y) (2)$$

$$at \qquad |y| = A: \mathbf{u}(\mathbb{p},t) = 0 \qquad (3)$$

$$at \qquad z = 0,2h: \mathbf{u}(\mathbb{p},t) = 0 \qquad (4)$$

for every $\mathbb{p} \in \partial\Omega$, **n** being a unit normal vector at $\mathbb{p}$, and $f(y)$ is a singularity function [11] called the unit ramp starting at $y|_{A/2} = \sigma$.

III. Experimental Approach

The employed loading system could produce only compression forces; we need to carry out a new system in order to generate the wanted load on $\partial\Omega$. Figure 2 illustrates the procedure that the authors propose to produce the same system as shown in Fig. 1. If a plate is subjected to a central load, as illustrated in Fig. 2a, the bending stresses are of equal magnitude at the top and bottom of the beam (compression at the top and tension at the bottom). The stress distribution over the cross section is shown in Fig. 2a (right). In order to have a stress from a constant value σ (top) to a constant value σ_{max} (bottom) at the plate, a rectangular groove was made long enough to have a shorter plate below the groove, as shown in Fig. 2b.
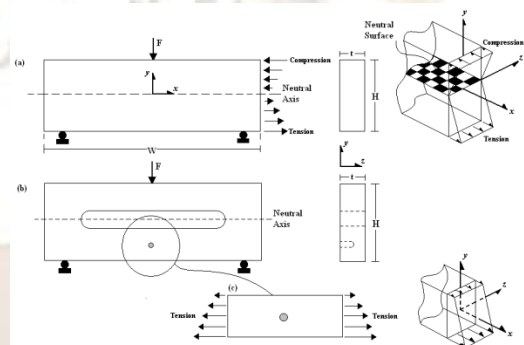

Figure 2 Stress distribution diagrams in the plate with the groove and acting load.

The shear force has the constant magnitude $F/2$ between the load and each support. The shear stress is maximum at the mid-height of the plate and decreases parabolically as it reaches the bottom of the plate; in coordinates,

$$\left(\tau_{xy}\right)_{max} = \frac{F/2}{2(tH^3/12)}\left[\left(\frac{H}{2}\right)^2 - y_1{}^2\right] (5)$$

The bending and shear stresses are of comparable magnitude if and only if W and H are of the same magnitude. Since for this particular problem $W = 280 \text{ mm} (10.9 \text{ in})$, $H = 62 \text{ mm} (2.4 in)$ from [11]

$$\frac{\left(\tau_{xy}\right)_{max}}{\left(\sigma_x\right)_{max}} = \frac{1}{2}\frac{H}{W} (6)$$

the ratio between the maximum bending and shear stress in the plate will be 17.5:1 respectively.

Having the groove offers one particular advantage: block the way of every fringe pattern produced by the loading cell so we can isolate the part under tension that is the analyze one.

Once the rectangular groove was made, a blind-hole at the mid-height and mid-width of the plate was drilled. Finally there is a plate with a centered circular blind-hole subjected to a non-uniform tensile load as shown in Fig. 2c and Fig. 1.

IV.   Experimental Method

Stress freezing method was used to determine the stress distribution in the transversal and longitudinal planes at blind-hole´s neighborhood. Once the slices were obtained, a circular polariscope was employed to analyze the fringe patterns.

As shown in the Fig. 3, transversal and longitudinal slices were cut out from the plate to be analyzed separately. Circular polariscope was used because the circular polarization eliminates isoclinics (loci of points of constant inclination of the principal axes of refraction).

Model Fabrication

A $508 \times 508 \times 9.6$ mm$(20 \times 20 \times 0.38$ in$)$ commercial photoelastic sheet, PSM-9, was supplied by Photoelastic Division of Measurements Group, Inc. The room- temperature stress-optic coefficient, C, for PSM-9 is nominally 10.5 kPa/$fringe/m$.

At the stress-freezing temperature of $110°C$ to $120°C (230°F$ to $250°F)$, the stress-optic coefficient is approximately 0.50 kPa/$fringe/m$ [10].

Eighteen $280 \times 62 \times 9.6$ mm$(11.02 \times 2.44 \times 0.38$ in$)$ pieces were cut out from the commercial sheet. A blind-hole of 4.8 mm$(3/16$ in$)$ in diameter with three $3.175, 6.41$ and 7.9 mm$(1/8, 1/4, 5/16$ in$)$ different depths was drilled at 140 mm $(5.5$ in$)$ from the right side and 13 mm$(0.51$ in$)$ from the bottom of the plate. A $90 \times 7.9 \times 9.6$ mm$(3.5 \times 0.31 \times 0.38$ in$)$ rectangular groove was drilled at 40 mm 1.57 in from the left side and 31 mm 1.22 in from the bottom of the plate, as in Figure 2b.

All the pieces were cut out from the commercial sheet with a band-saw operated at medium speed. The groove was made with an end mill with two fluted solid-carbide milling cutters with spiral flutes. Blind hole was drilled with a carbide-tipped boring tool at a medium speed (1280 rpm).

Loading Conditions

Two fasteners were made of aluminum alloy, 2070-T6, with mechanical properties: $E = 72$ GPa$(10.34$ Mpsi$)$, $\nu = 0.32$ to support the plate during the loading process. Loading was implemented by a load cell system instrumented with strain gages and a meter to read the force transmitted to plate.

The specimens were loaded at room temperature and subjected to a conventional stress-freezing cycle with a critical temperature of $115°C$ $(240°F)$.
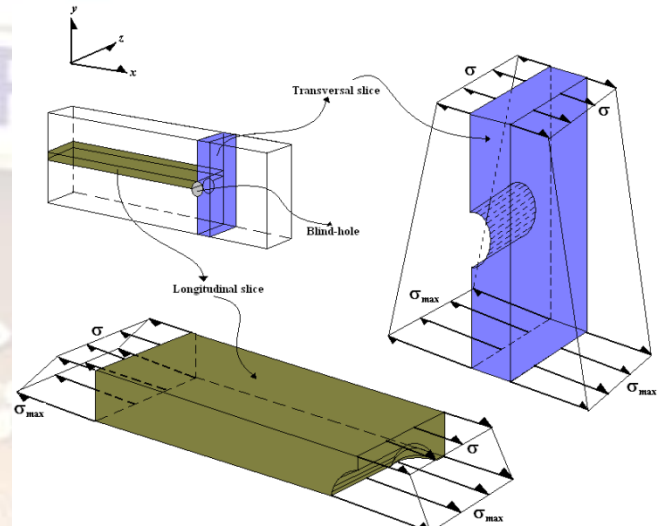

Figure 3 Slicing at the blind-hole´s neighborhood along planes of principal stress

A 950 N$(212.5$ lb$)$ force was produced by the cell load system to the plate once the critical temperature had been reach. The whole process was performed exactly as Dally and Riley [7] appoint.

After stress freezing, the model was rough cut on a band saw and ground to a final thickness of: i)3.1 mm$(0.23$ in$)$ for cross-sectional slice, and ii)2.9 mm$(0.11$ in$)$ for longitudinal slice. Air jet-cooling was used to prevent local heating.

Finite Element Analysis

This study was performed using the finite element code ABAQUS 6.7-1 [12]. The finite element model was built with the same finite element code and the postprocessor used to view the results was ABAQUS/Viewer 6.7-1. A typical mesh of a plate with a circular blind-hole is shown in Fig. 4.

To apply the boundary conditions, three areas were created to suffice this requirement. A first one of 1.5×9.6 mm$(0.06 \times 0.38$ in$)$ to apply constant pressure. Then the second and third ones of 1×9.6 mm$(0.04 \times 0.38$ in$)$ were created to apply displacement restrictions about *y* and *z* axis.

The plate is divided into two parts: a rectangle corresponding to the one containing the blind-hole,

by, J. Carrera, J.E. Martínez and L. Ferrer / International Journal of Engineering Research
and Applications   (IJERA)   ISSN: 2248-9622   www.ijera.com
Vol. 3, Issue 1, January -February 2013, pp.1017-1022

shown in the Fig. 2c with a finer mesh surrounding the blind-hole and the second part corresponding to the rest of the plate with a coarser mesh. 48 elements were used around the blind-hole.

Before the photoelastic stress-freezing test was performed a finite-element solution was obtained for the case of uniform pressure on the outer boundary (top rectangle) using the mechanical properties of the photoelastic material under stress-freezing conditions. The main purpose of this analysis was to estimate the amount of load to be applied on the model and to obtain an estimate of the displacements.
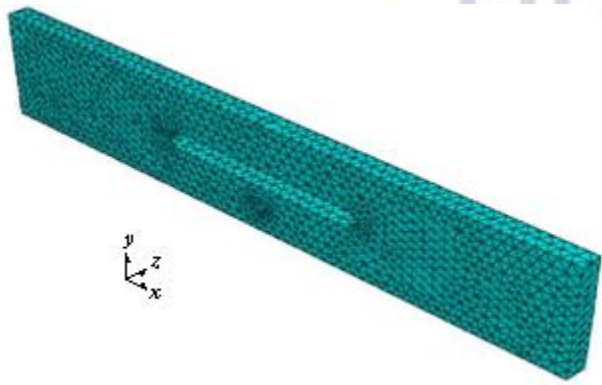

Figure 4 Typical mesh of a thin plate with a circular blind-hole presence

Experimental and Numerical Results

Figure 5 shows the loci of points considered in this study for transversal and longitudinal slices.

Transversal Slices

Figure 6 shows photoelastic results on the plate subjected to $981\,\text{N}(220.2\,\text{lb})$ load. On close evaluation we can see that the high-stress concentrations lie on both the transition zone (point 7) and at the free boundary (point 11).

The stress plotted in Fig. 7 correspond to the maximum principal stress, in this case the tangential stress, at the blind-hole's boundary.

At the boundary, one of the two principal stresses vanishes, so, in coordinates

$$\sigma_{\theta\theta} = \frac{Nf_\sigma}{h_1}\,(7)$$

where N is the fringe order, f_σ the material stress-fringe value and h_1 the slice thickness.

Figure 7a, 7b and 7c shows the FEManalysis results. The maximum stress occurs at points 10 and 11, with magnitudes of $25.6\,\text{MPa}(3.70\,\text{ksi})$ and $28.3\,\text{MPa}\ (4.09\,\text{ksi})$ respectively for the first case.

For the second and third cases it is more evident that the maximum stress occurred all along the blind-hole's route, having his higher value at points $8\left(31.92\,\text{MPa}(4.61\,\text{ksi})\right)$ and $11\left(34.22\,\text{MPa}(4.95\,\text{ksi})\right)$.
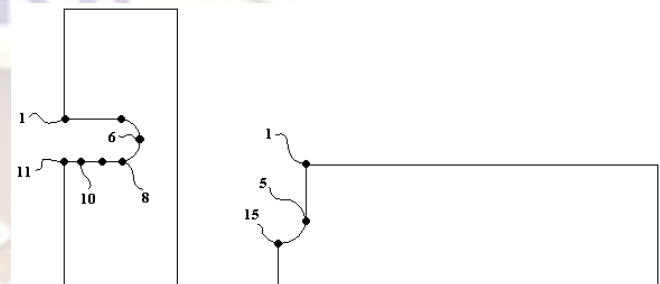

Figure 5 Loci of points considered for each slice

From Figure 7 one can conclude that the fringe pattern indicates that the stress is more uniformly distributed over the thickness when the blind-hole´s depth is $6.4\,\text{mm}(0.25\,\text{in})$ than the other two cases.

From Figure 7c it is interesting to notice that point 8 has slightly higher stress value than point 11 $\left(34.1\,\text{MPa}(4.93\,\text{ksi})\ versus\ 32.81\,\text{MPa}(4.74\,\text{ksi})\right)$.

Longitudinal Slices

Photoelastic results for longitudinal slices are shown in Figure 6d, 6e and 6f. They illustrate how the stress concentration lies at point 15 (root) for all depths. Figure 8 shows more evidently this fact: a longitudinal slice from a plate with a $4.6\,\text{mm}(0.19\,\text{in})$ circular blind-hole deepness under a $2107\,\text{N}(473\,\text{lb})$ load. The fringe pattern tends to concentrate at point 15.
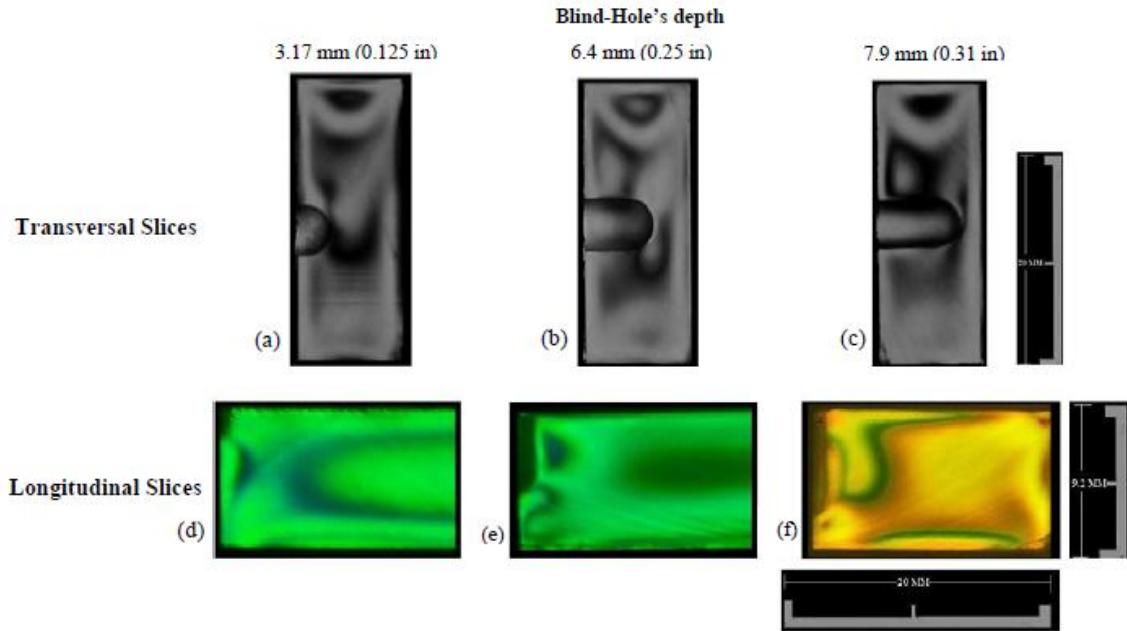
Figure 6 Photoelastic patterns, shown for representative transversal and longitudinal slices for three plates subjected to a 981 N (220.2 lb) load each one
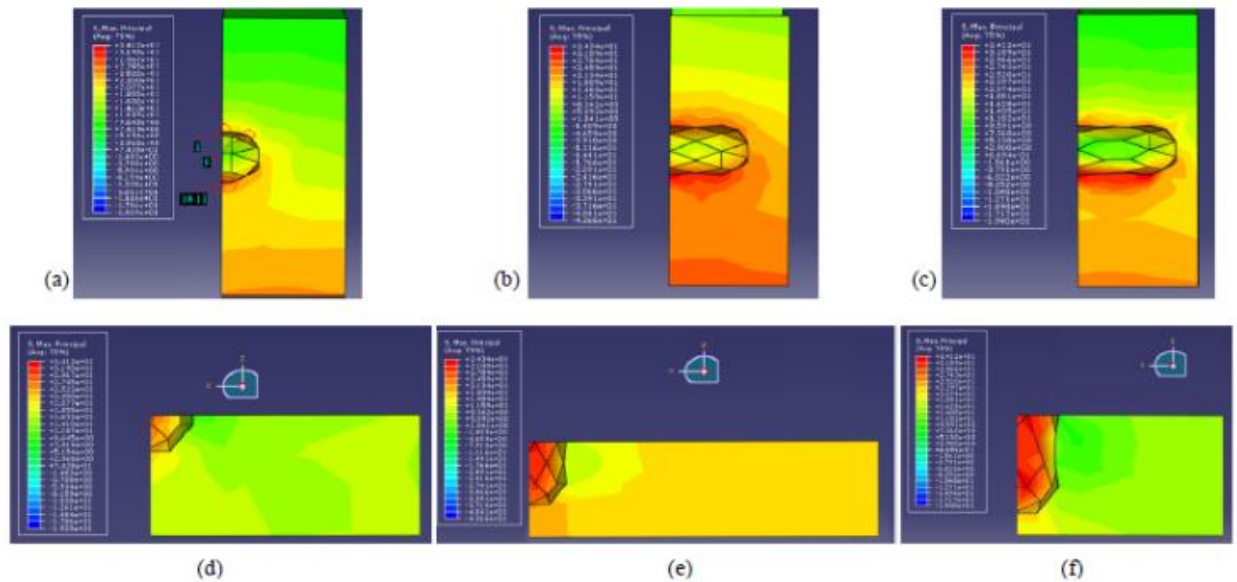

Figure 7 Distribution of maximum principal stress around the blind-hole under a 937 N (210 lb) load. First column corresponds to the transversal and longitudinal slices (3.1 mm depth); second and third columns are their similar for 6.4 mm and 7.9 mm blind-hole's depth respectively

Durelli and Riley [16, pp. 212-215] found that maximum stress for a strip with U-Shaped notches under axial load occurs at the center line of the notch with a deviation angle ϕ. Rubayi and Taft [9] also obtained the same locus for the maximum stress for a thick bar with U-Shaped notches.

The higher stress was 24.1 MPa(3.48 ksi) for the second case (blind-hole´s depth of 6.4 mm (0.25 in)).

The difference obtained by photoelasticity and FEM for stress values are about 15-20%. Taking into consideration that photoelastic methods provide results within a margin of uncertainty of 2.5 MPa(0.36 ksi) this is a reasonable result.

Discussion and Conclusions

Several experimental and numerical results were obtained to analyzed and evaluate the behavior of blind-holes in thin plates. The main interests of this study were stress concentration fields along the

root's concavity and along blind-hole's route under non-uniform tension loads.

For the transversal slice, experimental and FEM results showed that the maximum stress fields occurred when blind-hole's depth was 7.9 mm(0.31 in) and were located at points 8 and 11 (transition zone and at the free boundary plane respectively). The difference between both stresses is less than 3%. The fact that the maximal stresses were almost of the same magnitude at two points was significant. The finding demonstrates the importance of knowing that a possible failure (i.e. crack) may occur at either point, and not necessarily at point 11 where the experimentalist normally could reach.

For longitudinal slices, experimental results provide better qualitative understanding of the stress fields at the blind-hole's boundary.

The maximum stress occurs at point 15 (root's center) as can be seen in Figure 7. The numerical results matches the fringe pattern obtained via photoelastic method.

The experimental array in order to produce the requiring load for this study worked as well as we could expect for. For the cases when it was difficult to obtain qualitative results from experimental slices, the FEM is a very practical way to support them.

It has been proven that the deeper the blind-hole is, stress at points 8 (for transversal slice) and 15 (for longitudinal slice) must be considered.

Figure 8 shows the stress concentration factor behavior along blind-hole's boundary. These results should give for a scientist and engineer better and reliable information of what happens inside the hole and be aware of any possible failure.

After 17 iterations, FEM results converged within the expected results.
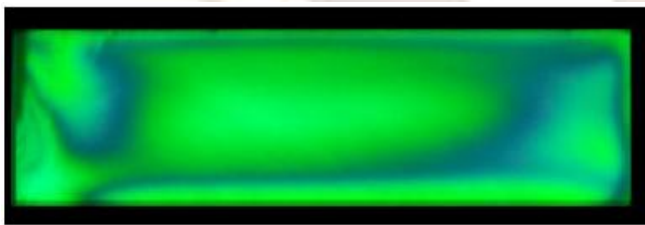

Figure 8 Shear stress fringe patterns for a longitudinal slice with 2107 N (474 lb) load

Acknowledgments

References

1. Kirsch, G., "Die Theorie der Elastizitat und die Bedürfnisse der Festigkeitslehre," Z. VereinesDeutscherIng., *42*, 797-807 (1898).
2. Iancu, F., Ding, X., Cloud, G. L., Raju, B. B., "Three-dimensional Investigation of Thick Single-lap Bolted Joints," Experimental Mechanics, *45* (4), 351-358 (2005).
3. Wang, W. C., Chen, Y-M., Lin, M-S., Wu, C-P., "Investigation of the Stress Field of a Near-surface Circular Hole," Experimental Mechanics, *45* (3), 244-249 (2005).
4. Peindl, R.D., Harrow, M. E., Connor, P.M., Banks, D.M., D'Allesandro, D.F., "Photoelastic Stress Freezing Analysis of Total Shoulder Replacement Systems," Experimental Mechanics, *44* (3), 228-234 (2004).
5. Gurtin, E. M., "An Introduction to Continuum Mechanics, First ed.," Academic Press, New York (2003).
6. Durelli, A. J., Phillips, E. A., Tsao, C. H., "An Introduction to the Theoretical and Experimental Analysis of stress and Strain, First ed.," McGraw-Hill Book Co., New York (1958).
7. Dally, J. W., Riley, W. F., "Experimental Stress Analysis, Fourth ed.," College House Enterprises LLC, Knoxville, TN (2005).
8. Cernosek, J., "Three-dimensional Photoelasticity by Stress Freezing, " Experimental Mechanics, *20,* 417-426 (1980).
9. Rubayi, N. A., Taft, M. E., "Photoelastic Study of Axially Loaded Thick-notched Bars," Experimental Mechanics, 377-383 (October 1982).
10. Vishay Measurements Group Inc., Photoelastic Division: Instruction Bulletin IB-242, Raleigh, NC (1996).
11. Crandall, S. H., Dahl, N. C., Lardner, T. J., "An Introduction to the Mechanics of Solids, Second ed.," McGraw-Hill International Book Co., New York (1978).
12. ABAQUS, Inc., "ABAQUS user's manual-version 6.7-1," Pawtucket, RI, USA (2008).
13. Gurtin, E. M., "The Mechanics and Thermodynamics of Continua, First ed., " Cambridge Press, London (2010).
14. Muskhelishvili, N. I., "Some Basic Problems of the Mathematical Theory of Elasticity, Second ed.," Noordhoff, Ltd., Groningen, Netherlands (1963).
15. Frocht, M. M., "Photoelasticity," Vol. II, John Wiley & Sons, New York (1948).
16. Durelli, A. J., Riley, W. F., "Introduction to Photomechanics," Prentice Hall(1965)